ALKALI ACTIVATION OF FLY ASH. PART III: EFFECT OF CURING CONDITIONS ON REACTION AND ITS GRAPHICAL DESCRIPTION

M. Criado[1], A. Fernández-Jiménez[2], A. Palomo[2]

[1]National Centre for Metallurgical Research (CSIC), Avda. Gregorio del Amo 8, 28040, Madrid, Spain

[2]Eduardo Torroja Institute (CSIC), Serrano Galvache 4, 28033, Madrid, Spain

Abstract

The micro- and nanostructural characteristics of the reaction products of fly ash alkali activation depend, among others, on the curing conditions used: temperature, time and relative humidity. The present study focuses primarily on relative humidity. When the material is cured in air-tight containers, the silicon content of the initial aluminium-rich material gradually increases. This end product is dense and compact. When samples are in direct contact with the atmosphere, however, early age carbonation takes place, resulting in water loss and persistence of a high aluminium content. This resulting material is granular and develops lower mechanical strength than the paste cured under high RH conditions. The main nano- and microstructural differences observed in the materials as a result of different curing conditions have been shown ~~to~~ through a graphical description of the reactions.

Keywords: Alkali activated; fly ash; relative humidity; microscopic and nanostructural model

* Corresponding author, Tel.: +34 91 553 8900; Fax: +34 91 534 7425; E-mail Address: mcriado@cenim.csic.es (M. Criado)

1. Introduction

The alkali activation of fly ash is a chemical process in which the ash is mixed with certain alkaline activators and cured at a mild temperature to generate compact solids **[1]**. Very broadly, the activation process can be viewed as a series of destruction-condensation reactions in which initially unstable structural units subsequently form coagulated structures able to condense into the hydrated products (alkaline aluminosilicate hydrate, N-A-S-H gel) **[2]**.

A number of models have been proposed in the literature to explain the formation of alkaline inorganic polymers (AIP). These models are based on results obtained with a variety of characterization techniques **[2-5]** and the existing knowledge about both silicate polymerization **[6]** and zeolite synthesis **[7,6]**. In 2005 A. Fernández-Jiménez and A. Palomo **[9,10]** proposed an updated version of the reaction mechanisms governing the alkali activation of aluminosilicates. Further to this model, the contact between the solid particles (aluminosilicates) and the alkaline solution induces the dissolution of the vitreous or amorphous component of the former, releasing (probably monomeric) aluminates and silicates. These monomers inter-react to form dimers, which in turn react with other monomers to form trimers, tetramers and so on. When the solution reaches saturation a N-A-S-H gel precipitates. Initially, this gel is an aluminium-rich aluminosilicate gel (Gel 1) **[11]**. Gel 1 formation may be explained by the higher Al^{3+} ion content in the alkaline medium in the early stages of the process (from the first few minutes to the first 4 to 5 hours). This, in turn, can be attributed to the fact that Al-O bonds are weaker and therefore more readily severed than Si-O bonds, making reactive aluminium more readily soluble than silicon **[7]**. As the reaction progresses, more Si-O groups in the solid particles dissolve, raising the silicate concentration in the medium. This ~~zeolite precursor~~ gel gradually becomes richer in silicon, giving rise to a N-A-S-H gel, called Gel 2 **[11].**

The most prominent of the many parameters playing a role in N-A-S-H gel synthesis include the nature of the starting materials, the nature and concentration of the alkali activator and the curing conditions.

In prior research, A. Palomo et al. **[4]** observed that mechanical strength rose exponentially with temperature, substantially reducing the time needed to reach a certain value. They also reported the existence of time and temperature threshold values,

however, at which mechanical strength rises more slowly, or may even decline. Temperature has also been observed to significantly affect the structural transition from the amorphous to the crystalline state in synthesized mineral polymers. Using XRD, P. Duxson **[12]** showed that even moderate rises in synthesis temperature led to visible increases in crystallinity in a polymer derived from metakaolin. Similarly, other authors have observed that in alkaline media the hydrothermal reaction may lead to the formation of semi-crystalline or polycrystalline phases **[13-15]**. The content of these (generally zeolite) phases grows with activation time **[3]**.

In addition to curing time and temperature, relative humidity has been shown to play a role in the initial curing of alkali-activated fly ash cement. A study by M. Criado et al. **[16]** stressed the importance of using suitable relative humidity, for the rapid carbonation that may otherwise take place slows the rate of ash activation and the development of mechanical strength in the end product. G. Kovalchuk et al. **[17]** showed that curing conditions determine the amount of water available during the hardening of alkali-activated fly ash matrices.

In light of the technological relevance of curing conditions, then, further study of this aspect, in particular the effect of ambient relative humidity on alkaline activation, is fully justified. In addressing this question, the present study aims primarily to determine how the composition of the product of fly ash alkali activation and its nanostructure are affected by relative humidity and how these changes impact its physical and mechanical properties.

2. Experimental

2.1. Materials

The chemical composition of the Spanish fly ash used in the present study, acquired from the Compostilla power plant (Class F, ASTM C 618-03), is given in Table 1. A much more exhaustive characterization of the ash was reported by the authors in a prior paper **[18]**.

Table 1.- Chemical analysis of the original fly ash

The ash was activated with an 8-M NaOH solution, prepared from ACS-ISO 98 % NaOH pellets supplied by Panreac S.A.

2.2. Method

The fly ash was mixed with the activating solution (liquid/solid ratio = 0.4) to prepare the pastes. The pastes were cured in an oven at 85 ºC for 8 hours, 20 hours, 28 and 60 days. Some of the activated ash specimens (1x1x6-cm prisms) were tested for standard cement strength (as per European code EN 196-1) at those ages. The curing procedures summarized below were the same as used in Part I of this study **[16].**

-Method 1: the moulds containing the paste were placed in air-tight containers with a small amount of water (relative humidity >90 %). The containers were then stored in an oven at 85 ºC.

-Method 2: the moulds were placed directly in the oven at 85ºC alongside a porcelain capsule containing water (relative humidity ≈40-50 %).

After thermal treatment, the degree of reaction was determined by attacking the materials with 1:20 HCl (by volume) **[19]**. The HCl used to prepare the solution 1:20 was hydrochloric acid 37% PA-ACS-ISO. This procedure determines the percentage of reaction products (N-A-S-H gel and zeolites) generated at the different thermal curing times, which dissolve in the acid solution, and the percentage of unreacted ash, which remains in the insoluble residue. The dissolved fraction is a parameter that provides information on the degree of reaction (%).

The experimental process followed consisted on placing 1 g of the ground (to a powder, particle size <65 μm) hardened material (activated ash) in a 250-ml flask containing 1:20 HCl. The mix was stirred with a plastic rotor for 3 hours, after which it was filtered

(through filter paper with a pore size of 15-20 μm) and the insoluble residue was washed with deionised water to a neutral pH. The filter paper containing the residue was placed in a previously weighed platinum crucible, dried on a heat plate and calcined at 1000 ºC in a furnace for one hour. The percentage of the dissolved phases was deduced from the weight loss. The degree of reaction or "α"and "IR" or the insoluble residue were determined with equations I and II.

$$IR(\%) = \frac{P_{initial} - P_{final}}{P_{final}} x100 \qquad \textbf{[Ec. I]}$$

$$\alpha\,(\%) = 100 - IR\,(\%) \qquad \textbf{[Ec. II]}$$

where $P_{initial}$ is the initial weight of the sample; P_{final} is the final weight of the insoluble residue after the HCl attack and calcination at 1000 ºC; ***IR*** is the unreacted percentage of fly ash (insoluble residue) and α is the percentage of reaction product.

This was followed by microstructural and nanostructural studies of the products with XRD, SEM/EDX and MAS NMR. A PHILIPS PW 1730 diffractometer with CuKα radiation was used in this study, along with a JEOL 5400 electronic microscope fitted with an OXFORD LINK EDX microanalysis system (a total of 20 acquisitions were obtained from each sample for elemental analysis). The NMR studies were conducted with a BRUKER AVANCE-400 facility.

3. Results

Figure 1 shows the degree of reaction of the working materials (under the two thermal curing procedures) against thermal curing time. Degree of reaction rose steeply in the

Method 1 materials, whereas it barely varied with reaction time in the Method 2 materials.

Fig. 1. Degree of reaction vs curing time for two thermal curing systems

Figure 2, in turn, shows variations in compressive strength under the two working systems. The pastes cured at higher relative humidity (Method 1, moulds in air-tight containers) exhibited higher strength, even doubling the values found for the pastes cured at lower relative humidity. Mechanical strength rose visibly with curing time in Method 1 specimens, while it remained essentially flat in the Method 2 pastes.

Fig. 2. Mechanical strength vs curing time for two working systems

The diffractograms for all the alkali-activated materials studied, as well as for the initial fly ash, are reproduced in Figure 3. The diffractogram for the initial ash changed perceptibly when the ash was activated: the halo attributed to the vitreous phase of the original ash shifted slighted to higher 2θ values (2θ=25-40º). This change denotes the formation of an alkaline aluminosilicate hydrate (N-A-S-H gel), the primary reaction product **[3,19,20]**. The minority crystalline phases (quartz, mullite and magnetite) detected in the initial material remained apparently unaltered. Alkaline activation also generated new zeolite-type crystalline phases. The type of these zeolites depended on the curing conditions: while with Method 1 hydrated sodalite ($Na_4Al_3Si_3O_{12}OH$, JCPDS 11-0401) and chabazite-Na ($NaAlSi_2O_6$ $.3H_2O$, JCPDS 19-1178) crystallized, only hydrated sodalite was detected in the Method 2 specimens. Moreover, the latter procedure favoured the formation of alkaline bicarbonates.

Fig. 3. Diffractograms of alkali-activated fly ash cured under Methods 1 and 2

Figure 4 shows certain morphological and microstructural characteristics of Method 1 and 2 activated ash after 20-hour and 60-day curing. The presence of sodium

aluminosilicate hydrate, the gel that forms the cementitious matrix, can be observed alongside the spheres of unreacted ash in these micrographs.

Fig. 4. Microstructure of the two systems studied: micrographs 1 and 2, cured under Method 1 for 20 hours and 60 days, respectively; micrographs 3 and 4, cured under Method 2 for 20 hours and 60 days, respectively

Table 2. Mean Si/Al ratios in N-A-S-H gels deduced from microscopical analysis.

After 20 hours, the Method 1-cured ash had a generally porous matrix. The degree of reaction in this system was moderate, with many fly ash spheres still practically intact. Curing time proved to be an essential factor in the acquisition of mechanical consistency (Figure 4(2)) and favoured the formation of small zeolite crystals (see Figure 4 (2a)). The main reaction product, N-A-S-H gel, became more silicon-rich over time, attaining an Si/Al ratio of 1.99 after 60 days (Table 2).

The 20-hour micrograph of the Method 2 material showed a very porous, scantly compact matrix, with a great many unreacted ash particles apparently (more than in the Method 1 material). In terms of reaction kinetics, this can be interpreted as follows. The matrices prepared pursuant to Method 2 developed more slowly than the Method 1 specimens. In the former, curing time did not appear to significantly affect the microstructure of the material, for the reaction barely progressed between 20 hours and 60 days. Consequently, the matrix was less developed than in the Method 1 material. The presence of the alkaline bicarbonates detected in this system (Figure 4(4b)) caused the material to develop a "granular" morphology in which the ash particles were partially attacked but conserved their initial spherical geometry. This same morphology has been observed in other alkaline cementitious systems when carbonates are added to the medium **[21]**. Moreover, no zeolites were observed in these matrices, which were scantly crystallized, as confirmed by XRD. Furthermore, the N-A-S-H gel forming in this system had a lower Si/Al ratio than the Method 1 material (see Table 2).

In the nanostructural study of the materials, the ^{29}Si spectrum of the original ash was found to be characterized by a very wide and scantly defined signal, indicative of the

heterogeneous distribution of the silicon atoms (Figure 5). The peaks identified at -80, -84, -95, -100, -104 and –109±1 ppm were associated mostly with the vitreous phase forming part of the material **[18]**.

Some of these signals (-80, -95 and -100 ppm) were observed to disappear on the ^{29}Si spectra of the alkali-activated pastes cured for 8 hours with the Method 1 procedure (Figure 5(1)). Very intense peaks also appeared on these spectra at -88.2, -93.2 and -98.5 ppm, along with lower intensity signals at -103.5 and -109.2 ppm, located in positions close to the ones detected for the silicon in certain zeolites **[8,22]**. These five signals were attributed to silicon atoms respectively surrounded by Al_4, $SiAl_3$, Si_2Al_2, Si_3Al and Si_4. The position of the signals did not vary significantly with increasing curing time (60 days), although peak resolution and intensity changed substantially. In the 8-hour spectra, the most intense signals were observed at -88.2, -93.2 and -98.5 ppm. The peak whose intensity grew most with curing was the one at -98.6 ppm. These differences in intensity can be associated with variations in the composition of the sodium aluminosilicate hydrate over time. At 8 hours the gel formed, Gel 1, had a high aluminium content **[11]**, with a predominance of $Q^4(4Al)$, $Q^4(3Al)$ and $Q^4(2Al)$ units. With time, the silicon content of this reaction product grew **[11]**, whereby $Q^4(3Al)$ and $Q^4(2Al)$ units prevailed (signals at -93.3 and -98.6 ppm, respectively).

Fig. 5. ^{29}Si MAS NMR spectrum for alkali-activated Method 1 and Method 2 pastes

The 8-hour ^{29}Si spectrum for the material cured at low relative humidity (Figure 5(2)) contained an intense peak at -87.5 ppm, along with another series of signals at -100.3, -105.9 and -111.0 ppm. These latter three signals, attributed to the vitreous phase in the starting material, indicated that the ash had barely reacted with the alkaline solution. The signal at -87.5 ppm, in turn, was associated with the presence of $Q^4(4Al)$ units, apparently denoting the formation of an aluminium-rich reaction product (Gel 1). The area of this signal was greater than in the 8-hour spectrum for the Method 1 material. The shape of the spectra barely changed with time (60 days): nonetheless, the intensity of the signals at -100.8 and -105.5 ppm declined slightly, which, together with the appearance of a signal at -93.5 ppm, provided evidence that the fly ash was gradually reacting. This spectrum exhibited much lower resolution than the 60-day spectrum for the high relative humidity material and bore a closer resemblance to the 8-hour findings

for Method 1. All of the foregoing confirms that unsuitable curing conditions may have a perceptible effect on fly ash activation reaction kinetics.

4. Discusión

Carbonation depends on the facility with which carbon dioxide can penetrate the pores of a material. Relative humidity plays a fundamental role in carbon dioxide diffusion, for the diffusion coefficient of CO_2 in air is ten times higher than in water. G. Verbeck **[23]** showed that carbonation is favoured when relative humidity lies within the critical range of 60-70 %.

Consequently, curing alkali activated materials at a relative humidity of over 90 % (Method 1) ensures pore saturation. Acording to previous works **[24,25]** and Kelvin-Laplace equation all pores are saturated with water except to pores above ≈ 10 nm in radius, justifying a weak CO_2 penetration, rendering carbonation practically nil. Under these conditions, the excess of available water and a high pH favoured dissolution of the vitreous component of the fly ash, stimulating the activation reaction and yielding a well developed material, mechanically speaking.

Water is a good reaction medium because solid aluminosilicate dissolution via alkaline hydrolysis consumes water. A certain amount of excess water is therefore needed to dissolve aluminate and silicate species. In a medium with high relative humidity the aluminate and silicate species are rapidly taken up in the aqueous phase and N-A-S-H gel begins to precipitate when saturation is reached. The water nominally consumed during dissolution is released in this condensation process. As a result, the time needed for a supersaturated aluminosilicate solution to form a continuous gel varies considerably with the curing conditions.

N-A-S-H gel must be regarded to be a zeolite precursor which over time gives rise to crystalline zeolites **[3]**. Zeolite stability is affected by the presence of chemical species such as water or organic molecules in zeolite cavities **[26]**. Regardless of their nature, these molecules lower the chemical potential of the zeolite and stabilize its structural grid. In the material cured here at a relative humidity of over 90 %, the sodium cations that compensate for the charge deficit generated by the replacement of silicon with

aluminium are hydrated and enhance zeolite stability. This in turn favours the crystallization of these minerals (hydrated sodalite and chabazite-Na) and increases their presence with time.

By contrast, when cured at a relative humidity of ≈50 %, the materials are in a near critical situation in terms of carbonation. In such conditions, carbonation retards or halts the activation reaction, yielding a granular, porous and fairly weak product. The explanation for this change in reaction kinetics is that since the pores are not water-clogged, carbon dioxide molecules are able to penetrate and carbonate the material. Alkaline bases are known to carbonate rapidly when in contact with dissolved CO_2.

$$CO_2 + 2KOH\ (NaOH) \xrightarrow{H_2O} K_2CO_3\ (Na_2CO_3) + H_2O$$

In addition, curing in a medium with lower relative humidity where the amount of liquid water is somewhat scant retards the dissolution of the vitreous component of the fly ash (lower degree of reaction, see Figure 1). These conditions would appear to have a greater effect on silicate than aluminate species, for aluminium dissolves more readily than silicon **[7]**. That may also explain the precipitation under such circumstances of an aluminium-rich aluminosilicate hydrate (N-A-S-H gel) whose composition (silicon content) barely varies over time because the decline in pH induced by carbonation hinders subsequent silicon dissolution (see Figure 5(2)).

In such a low relative humidity system hydrated sodium cations are too scant to effectively favour zeolite stabilization. As a result, only hydrated sodalite forms (see Figure 3).

The graphic-kinetic model proposed below on the grounds of the data compiled in this study charts the evolution of the phases in the starting materials and the products forming during alkali activation (Figures 6 and 7).

As Figure 6 shows, the starting material consists solely in fly ash, mullite and magnetite. Alkali activation induces the precipitation of a N-A-S-H gel, several zeolite

species and alkaline bicarbonates (depending on the curing method). The same minority crystalline phases present in the original ash (quartz and smaller proportions of mullite) are detected throughout, along with a small number of fly ash spheres, some partially attacked.

Fig. 6. Microscopic model of the working systems: (1) high relative humidity curing method; (2) low relative humidity curing method

After 8 hours, the degree of reaction in the Method 1 material was 47.18 % compared to 39.84 % in the low relative humidity specimens. In other words, more N-A-S-H gel was generated in the former, where more ash reacted, than in the latter. The microstructure was similar in the two systems, with a porous and scantly compact matrix. Variation in matrix morphology with time depended on the curing method. When the material was cured under high relative humidity conditions, the end result was a dense, compact system and a strong matrix. By contrast, the microstructure of the system cured at a relative humidity of around 50 % remained practically unchanged after 60 days in the oven at 85 ºC, when its matrix still contained a fairly large number of pores and a series of unreacted ash spheres (degree of reaction = 42.15 %). Finally, in addition to N-A-S-H gel, zeolites were detected in both systems. The amount of hydrated sodalite and chabazite-Na, identified in the Method 1 system, grew with time. In the Method 2 system, alkaline bicarbonates and very small quantities of sodalite precipitated.

Figure 7 illustrates the dissolution of the vitreous structure of the fly ash when it came into contact with the alkaline solution (8-M NaOH). The dissolved species subsequently inter-reacted to form more intensely polymerized structures that precipitated as N-A-S-H gel when they reached saturation. This figure relates the variation in N-A-S-H gel structure and composition with time to the curing conditions.

Fig. 7. Nanostructural plotting of the systems studied: (1) high relative humidity curing method; (2) low relative humidity curing method

In the Method 1 material the dissolved species inter-reacted quickly, and after 8 hours yielded an aluminium-rich gel (Gel 1) with a predominance of $Q^4(4Al)$ and $Q^4(3Al)$ units. The silicon content in this gel gradually rose with reaction time (thermal curing

time). Since tetrahedral silicon tends to be surrounded by two or three aluminium atoms, the Si/Al ratio in the N-A-S-H gel grew (Si/Al ratio ≈ 2). This gel had a higher range structural order than the Method 2 material, as borne out by the higher resolution of the signals on the ^{29}Si spectra (see Figure 5(1)). By contrast, in the material cured under the low humidity conditions that favoured initial carbonation, water loss in the material and a decline in pH, the vitreous phase of the fly ash dissolved more slowly when in contact with the alkaline solution. The aluminium-rich compound (Gel 1) initially formed, with a prevalence of Q^4(4Al) and Q^4(3Al) units, was less intensely polymerized than in Method 1. This phase barely changed over time due to the pH conditions induced by carbonation. Consequently, after 60 days, both its chemical composition and structure remained essentially unchanged (Gel 1: with an Si/Al ratio = 1.64, where the silicon tends to be surrounded by three aluminium atoms and exhibit low range structural order, as reflected in the poor resolution of the signals on the ^{29}Si spectrum).

5. Conclusions

Curing conditions play a very important role in the micro- and nanostructural development of the reaction products obtained in fly ash alkaline activation.

Curing at a relative humidity of over 90 %, in which the pastes are kept in air-tight containers, yields a dense, compact material, whose initially high aluminium content gives way to silicon uptake and good mechanical development over time.

Curing at low relative humidity with the pastes in direct contact with the atmosphere generates a granular, porous material. The aluminium-rich reaction products are very stable, with a chemical composition that remains unchanged throughout the curing process, ultimately resulting in a weaker material.

Finally, a graphical description of the main nano- and microstructural differences observed in the materials as a result of employing thermal cured with different relative humidity conditions has been proposed.

Acknowledgements

This study was funded by MICINN under project MAT2006-11705. M. Criado express her gratitude to the CSIC for the contract under the JAE-Doc contract (ref. JAE-Doc2007) cofinanced by the European Social Fund.

References

[1] Palomo A, Gtutzeck MW, Blanco MT. Alkali-activated fly ashes: A cement for the future. Cement Concrete Res 1999;29:1323-9.

[2] Criado M, Fernández-Jiménez A, Palomo A. Alkali activation of fly ash. Effect of the $Si_{O2}/N_{a2}O$ ratio. Part I: FTIR study. Micropor Mesopor Mat 2007;106:180-91.

[3] Criado M, Fernández-Jiménez A, de la Torre AG, Aranda MAG, Palomo A. An XRD study of the effect of the SiO_2/Na_2O ratio on the alkali activation of fly ash. Cement Concrete Res 2007;37:671-9.

[4] Palomo A, Alonso S, Fernández-Jiménez A, Sobrados I, Sanz J. Alkaline activation of fly ashes: NMR study of the reaction products. J Am Ceram Soc 2004;87:1141-5.

[5] Provis JL, Van Deventer JSJ. Direct measurement of the kinetics of geopolymerisation by in-situ energy dispersive X-ray diffractometry. J Mater Sci 2007;42:2974-81.

[6] Iler RK. The chemistry of silica. New York: Wiley; 1979.

[7] Fernández-Jiménez A, Palomo A. Mid-infrared spectroscopic studies of alkali-activated fly ash structure. Micropor Mesopor Mat 2005;86:207-14.

[8] Engelhardth G, Michel D. High resolution solid state NMR of silicates and zeolite. London: Wiley; 1987.

[9] Fernández-Jiménez A, Palomo A, Alonso MM. Alkali Activation of fly ashes: Mechanisms of reaction. 2nd Inter. Symposium NON-TRADITIONAL CEMENT & CONCRETE; 2005, Brno, Czech Republic.

[10] Palomo A, Fernández-Jiménez A, Criado M, Alonso MM. The alkali activation of fly ashes: from macro to nanoscale. 2nd International Symposium on Nanotechnology in Construction; 2005; Bilbao, Spain.

[11] Fernández-Jiménez A, Palomo A, Sobrados I, Sanz J. The role played by the reactive alumina content in the alkaline activation of fly ashes. Micropor Mesopor Mat 2006;91:111-9.

[12] Duxson P. The structure and thermal evolution of metakaolin geopolymers. PhD Thesis; 2006; University of Melbourne, Australia.

[13] Duxson P, Fernández-Jiménez A, Provis JL, Lukey GC, Palomo A, van Deventer JSJ. Geopolymer technology: the current state of the art. J Mater Sci 2007;42:2917-33.

[14] Rowles M, O`Connor B. Chemical optimisation of the compressive strength of aluminosilicate geopolymers synthesised by sodium silicate activation of metakaolinite. J Mater Chem 2003;13:1161-65.

[15] Van Jaarsveld JGJ, van Deventer JSJ. The effect of metal contaminants on the formation and properties of waste-based geopolymers. Cement Concrete Res 1999;29:1189-200.

[16] Criado M, Palomo A, Fernández-Jiménez A. Alkali activation of fly ashes. Part 1: Effect of curing conditions on the carbonation of the reaction products. Fuel 2005;84:2048-54.

[17] Kovalchuk G, Fernández-Jiménez A, Palomo A. Alkali-activated fly ash: Effect of thermal curing conditions on mechanical and microstructural development-Part II. Fuel 2007;86:315-22.

[18] Fernández-Jiménez A, Palomo A. Characterisation of fly ashes. Potential reactivity as alkaline cements. Fuel 2003;82:2259-65.

[19] Fernández-Jiménez A, de la Torre AG, Palomo A, López-Olmo G, Alonso MM, Aranda MAG. Quantitative determination of phases in the alkali activation of fly ash. Part II. Degree of reaction. Fuel 2006;85:1960-69.

[20] Fernández-Jiménez A, de la Torre AG, Palomo A, López-Olmo G, Alonso MM, Aranda MAG. Quantitative determination of phases in the alkali activation of fly ash. Part I. Potential ash reactivity. Fuel 2006;85:625-34.

[21] Fernández-Jiménez A, Palomo A, Criado M. Alkali activated fly ash binders. A comparative study between sodium and potassium activators. Mater Construcc 2006;56:51-65.

[22] Klinowski J. Nuclear magnetic resonance studies of zeolites. Progress in NMR Spectroscopy 1984;16:237-309.

[23] Verbeck G. Carbonation of hydrated Portland cement. Cement and Concrete. ASTM STP 205, 1958: 17-36.

[24] Bentz DP, Quenard DA, Baroghel-Bouny V, Garboczi EJ, Jennings HM. Modelling drying and shrinkage of cement paste and mortar. Part 1. Structural models from nanometres to milimetres. Mar Strut 1995;28:450-8.

[25] Grasley ZC, Lange DA, D`Ambrosia MD. Internal relative humidity and drying stress gradients in concrete. Mar Strut 2006;39:901-9.

[26] García Martínez J, Pérez Pariente J. Materiales zeolíticos: síntesis, propiedades y aplicaciones. Alicante: Publicaciones de la Universidad de Alicante; 2002.

Figures

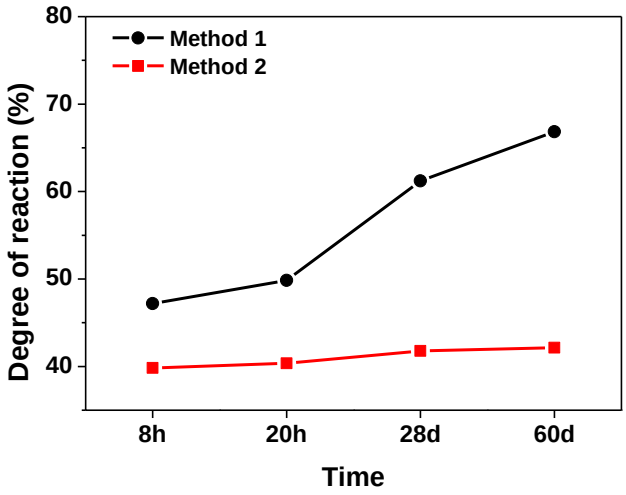

Fig. 1. Degree of reaction vs curing time for two thermal curing systems

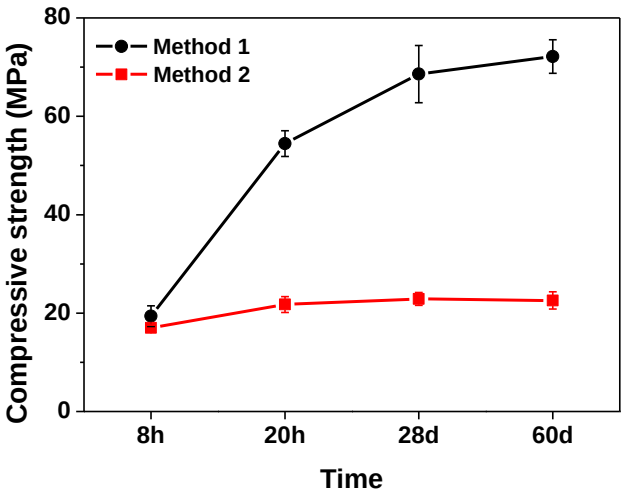

Fig. 2. Mechanical strength vs curing time for two working systems

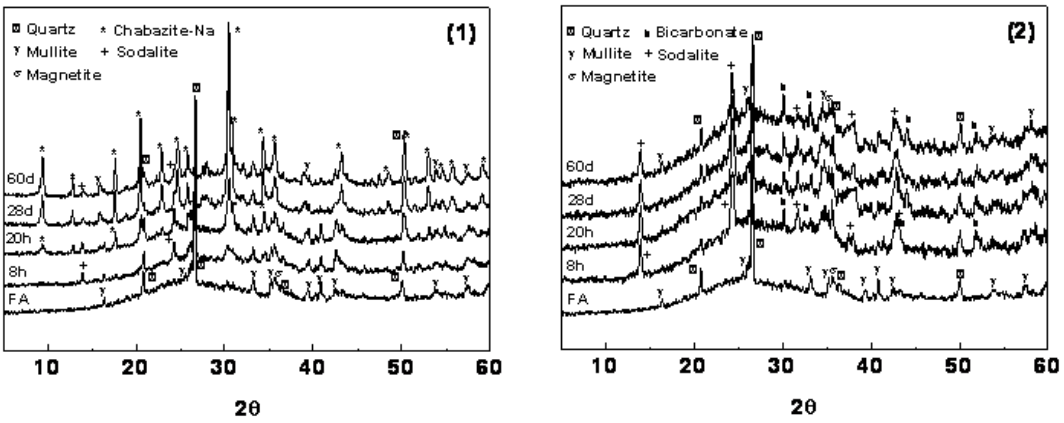

Fig. 3. Diffractograms of alkali-activated fly ash cured under Methods 1 and 2

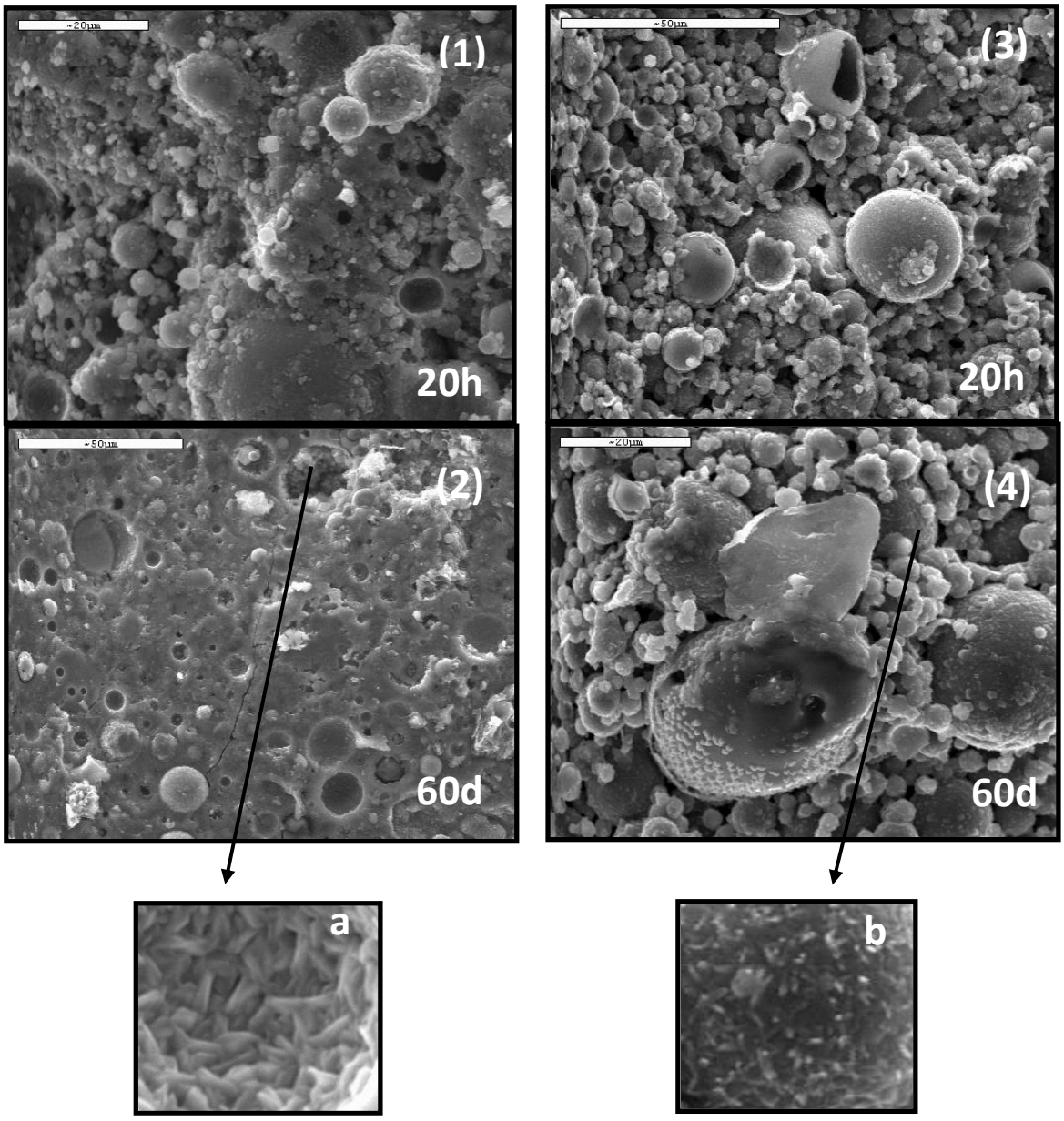

Fig. 4. Microstructure of the two systems studied: micrographs 1 and 2, cured under Method 1 for 20 hours and 60 days, respectively; micrographs 3 and 4, cured under Method 2 for 20 hours and 60 days, respectively

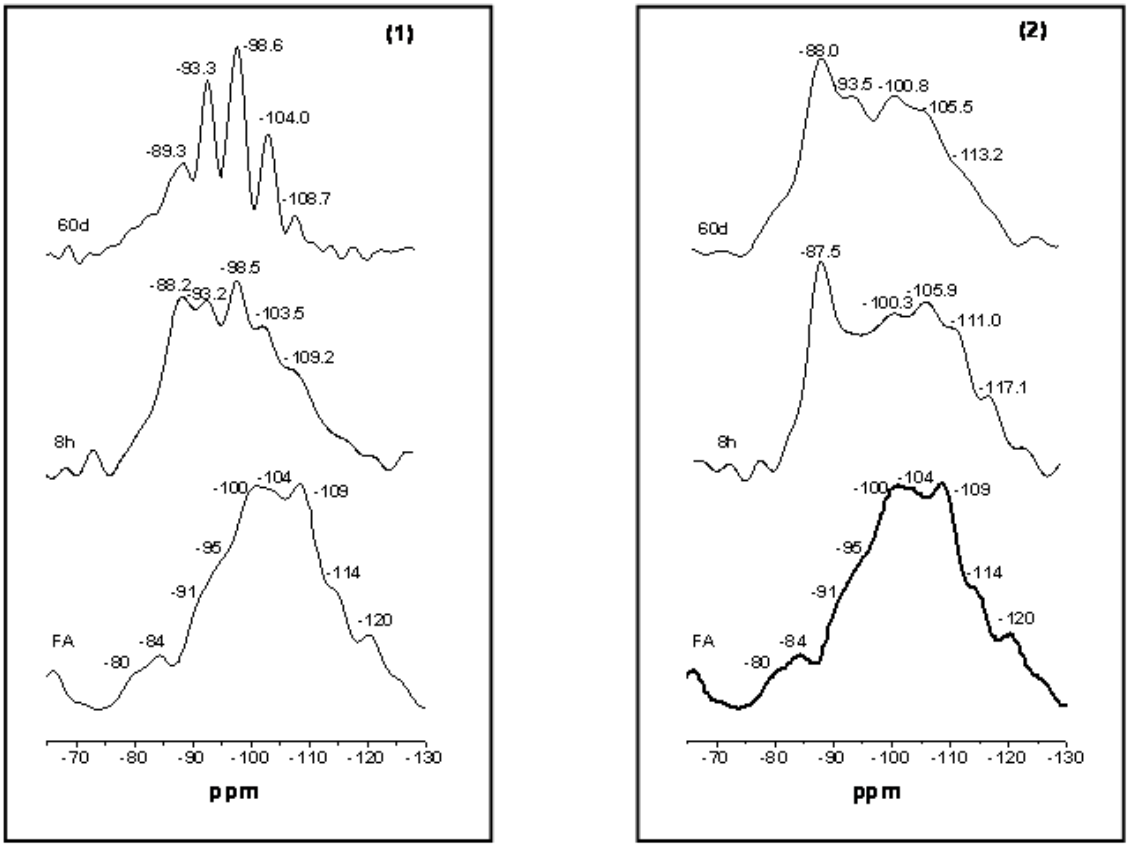

Fig. 5. ^{29}Si MAS NMR spectrum for alkali-activated Method 1 and Method 2 pastes

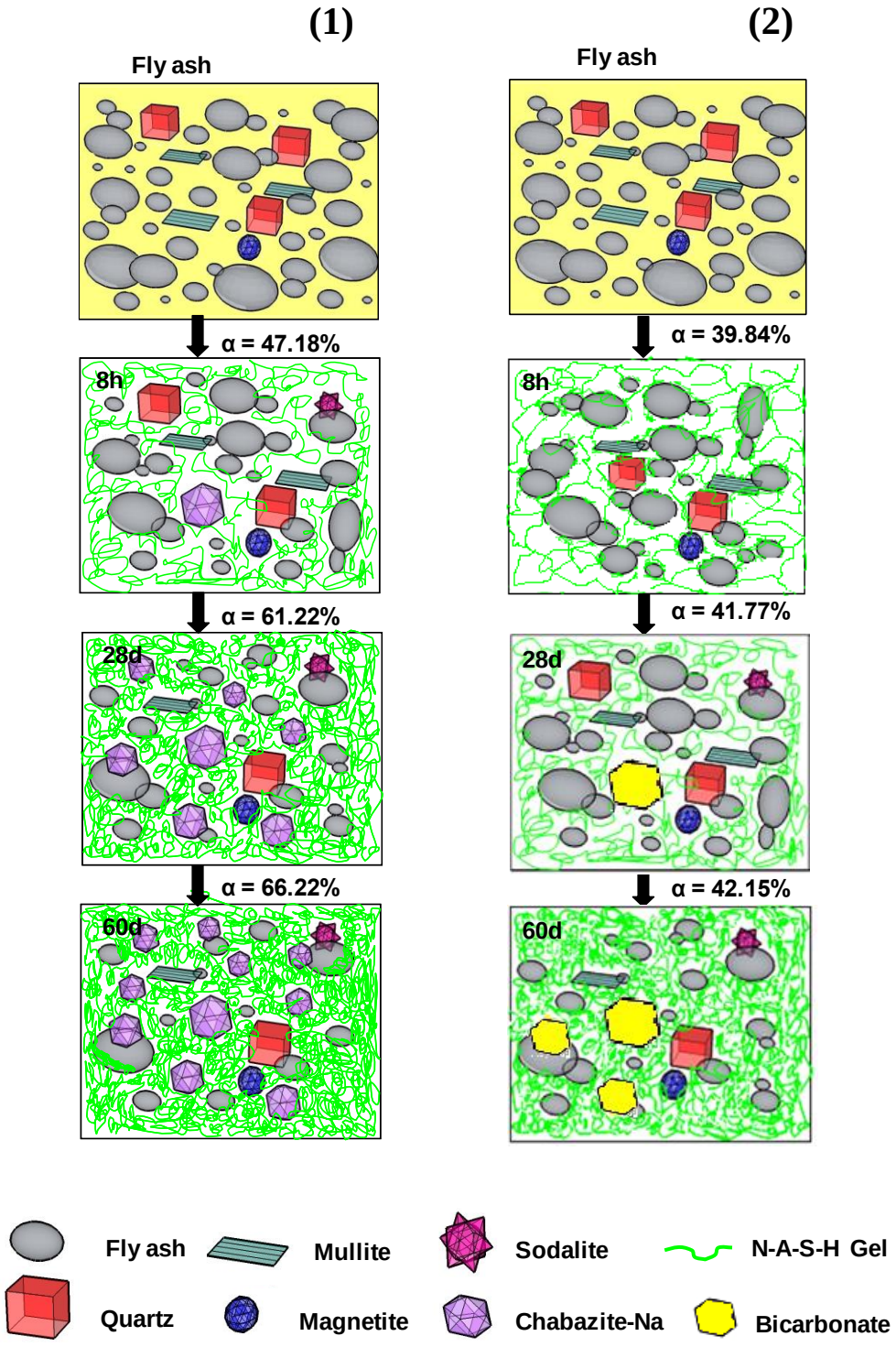

Fig. 6. Microscopic model of the working systems: (1) high relative humidity curing method; (2) low relative humidity curing method

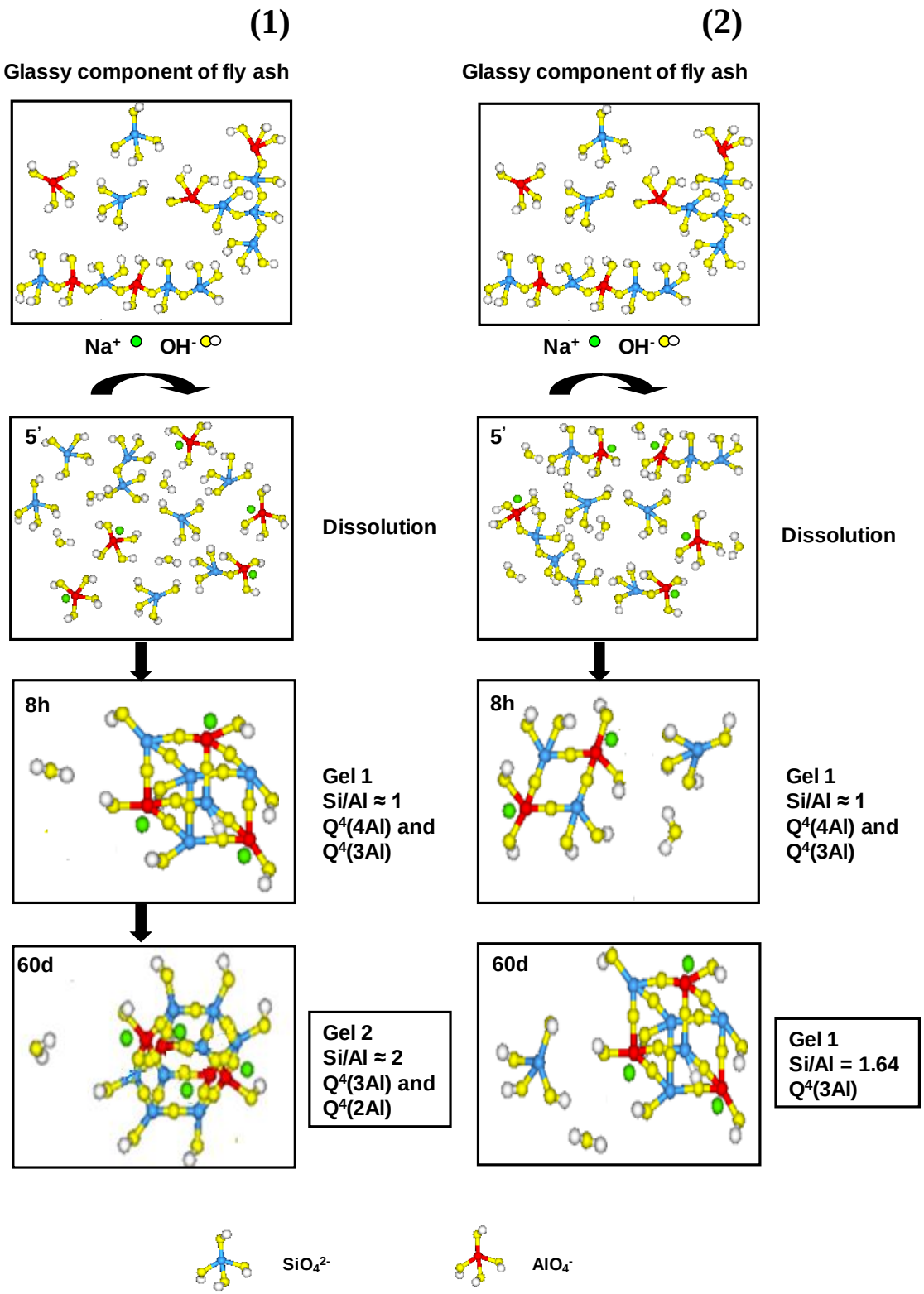

Fig. 7. Nanostructural model of the systems studied: (1) high relative humidity curing method; (2) low relative humidity curing method

Tables

Table 1. Chemical analysis of the initial fly ash (%)

Table 2. Mean Si/Al ratios in N-A-S-H gels deduced from microscopical analysis.

Table 1. Chemical analysis of the original fly ash

	L.I.	I.R.	SiO_2	Al_2O_3	Fe_2O_3	CaO	MgO	SO_3	K_2O	Na_2O	TiO_2	Total
%Wt	3.59	0.32	53.09	24.80	8.01	2.44	1.94	0.23	3.78	0.73	1.07	100

L.I. = loss on ignition; I.R. = insoluble residue

Table 2. Mean Si/Al ratios in N-A-S-H gels deduced from microscopical analysis.

	Si/Al (20h at 85°C)	**Si/Al (60d at 85°C)**
Method 1	1.88 ± 0.12	1.99 ± 0.08
Method 2	1.40 ± 0.09	1.68 ± 0.15